Crystal structure of human IRAK1

Li Wang[a,b], Qi Qiao[a,b], Ryan Ferrao[a,b], Chen Shen[a,b], John M. Hatcher[a,c], Sara J. Buhrlage[a,c], Nathanael S. Gray[a,c], and Hao Wu[a,b,1]

[a]Department of Biological Chemistry and Molecular Pharmacology, Harvard Medical School, Boston, MA 02115; [b]Program in Cellular and Molecular Medicine, Boston Children's Hospital, Boston, MA 02115; and [c]Department of Cancer Biology, Dana–Farber Cancer Institute, Boston, MA 02115

Edited by Jonathan C. Kagan, Boston Children's Hospital, Boston, MA, and accepted by Editorial Board Member K. C. Garcia November 7, 2017 (received for review August 14, 2017)

Interleukin 1 (IL-1) receptor-associated kinases (IRAKs) are serine/threonine kinases that play critical roles in initiating innate immune responses against foreign pathogens and other types of dangers through their role in Toll-like receptor (TLR) and interleukin 1 receptor (IL-1R) mediated signaling pathways. Upon ligand binding, TLRs and IL-1Rs recruit adaptor proteins, such as myeloid differentiation primary response gene 88 (MyD88), to the membrane, which in turn recruit IRAKs via the death domains in these proteins to form the Myddosome complex, leading to IRAK kinase activation. Despite their biological and clinical significance, only the IRAK4 kinase domain structure has been determined among the four IRAK family members. Here, we report the crystal structure of the human IRAK1 kinase domain in complex with a small molecule inhibitor. The structure reveals both similarities and differences between IRAK1 and IRAK4 and is suggestive of approaches to develop IRAK1- or IRAK4-specific inhibitors for potential therapeutic applications. While the IRAK4 kinase domain is capable of homodimerization in the unphosphorylated state, we found that the IRAK1 kinase domain is constitutively monomeric regardless of its phosphorylation state. Additionally, the IRAK1 kinase domain forms heterodimers with the phosphorylated, but not unphosphorylated, IRAK4 kinase domain. Collectively, these data indicate a two-step kinase activation process in which the IRAK4 kinase domain first homodimerizes in the Myddosome, leading to its *trans*-autophosphorylation and activation. The phosphorylated IRAK4 kinase domain then forms heterodimers with the IRAK1 kinase domain within the Myddosome, leading to its subsequent phosphorylation and activation.

interleukin 1 receptor-associated kinases | IRAK1 | crystal structure

Currently, four members of the IL-1 receptor-associated kinase (IRAK) family have been identified: IRAK1 (1), IRAK2 (2), IRAK3 (3) (also called IRAK-M), and IRAK4 (4). IRAK family members share a conserved domain architecture (Fig. 1*A*) consisting of an N-terminal death domain (DD) followed by either a C-terminal kinase domain (KD) (IRAK1 and IRAK4) or pseudokinase domain (IRAK2 and IRAK3). IRAK1 also contains a proline/serine/threonine-rich domain (ProST) in between the DD and the kinase domain while IRAK1, IRAK2, and IRAK3 have a C-terminal region important for the recruitment and activation of the downstream effector TNF receptor-associated factor 6 (TRAF6) (5).

IRAK1 was identified through coimmunoprecipitation with IL-1 receptor (IL-1R) (1). Signaling through IL-1Rs and most Toll-like receptors (TLRs) requires the adaptor myeloid differentiation primary response gene 88 (MyD88) (6). MyD88 is comprised of two protein–protein interaction domains, an N-terminal DD followed by a Toll/IL-1R homology (TIR) domain (7). Upon ligand-mediated receptor activation, MyD88 is recruited to TIR-containing receptors through homotypic TIR–TIR domain interactions. Subsequently, DD–DD interactions between MyD88 and IRAK4 facilitate the recruitment of IRAK4 to the receptor complex. Additional DD–DD interactions between IRAK4 and IRAK2, and possibly between IRAK4 and IRAK1, facilitate the formation of the MyD88/IRAK4/IRAK1 Myddosome (8, 9). The Myddosome complex functions to promote IRAK4 dimerization, *trans*-autophosphorylation, and activation (10). IRAK4 then phosphorylates IRAK1 to first prime its activity, enabling subsequent IRAK1 autophosphorylation in its activation loop to become fully activated (11).

Active IRAK1 undergoes further autophosphorylation, leading to hyperphosphorylation of the ProST region. This hyperphosphorylation induces IRAK1 to dissociate from the Myddosome and associate with the downstream effector TRAF6 (1, 12). TRAF6 activation and ubiquitination of IRAK1 trigger the initiation of a transcriptional program mediated by NF-κB and activator protein 1, leading to the induction of proinflammatory and immunomodulatory cytokines, such as IL-1β, TNF-α, IL-6, and IL-18. Additionally TLR7, TLR8, and TLR9 can induce IFN-α production in plasmacytoid dendritic cells upon viral infection (13, 14). TLR7- and TLR9-mediated IFN-α production requires the MyD88–IRAK4–IRAK1 complex, and both IRAK4 and IRAK1 kinase activities are essential (15).

To date several physiological substrates for IRAK1 have been clearly identified, including IRAK1 itself, the adaptor protein Tollip (16), the E3 ligase Pellino (17, 18), and the transcription factor IRF7 (15). Phosphorylation of IRAK1 and Tollip has been shown to weaken the IRAK1–Tollip interaction and promote the dissociation of IRAK1 from the Myddosome. IRAK1 can interact and phosphorylate Pellino proteins, which promotes Pellino-mediated polyubiquitination of IRAK1. The ubiquitin-binding domain of NEMO (also known as IKKγ) binds to polyubiquitinated IRAK1, bringing together the IRAK1–TGF-beta activated kinase 1 (TAK1)–TRAF6 complex and the NEMO-IKKα-IKKβ complex to activate NF-κB signaling (19, 20). IRAK1 can interact with and phosphorylate IRF7, leading to IRF7 translocation into the nucleus and induction of type I IFN gene transcription (15).

Significance

Innate immune signaling has an essential role in inflammation, and dysfunction of signaling components in these pathways contributes to autoimmunity and cancer. Interleukin-1 receptor-associated kinase (IRAK) family members are key mediators of signal transduction by Toll-like receptors and Interleukin-1 receptors in innate immunity and therefore serve as potential therapeutic targets for these diseases. The crystal structure of the IRAK1 kinase domain in complex with a small molecule inhibitor reveals important structural details of the kinase that provide insights into the design of selective IRAK inhibitors. Characterization of IRAK1 heterodimerization with the upstream kinase IRAK4 suggests a mechanism of IRAK1 activation by IRAK4.

Author contributions: L.W., R.F., and H.W. designed research; L.W., Q.Q., R.F., and C.S. performed research; J.M.H., S.J.B., and N.S.G. contributed new reagents/analytic tools; L.W., Q.Q., R.F., and H.W. analyzed data; and L.W., R.F., and H.W. wrote the paper.

The authors declare no conflict of interest.

This article is a PNAS Direct Submission. J.C.K. is a guest editor invited by the Editorial Board.

Data deposition: The atomic coordinates and structure factors have been deposited in the Protein Data Bank, www.wwpdb.org (PDB ID code 6BFN).

[1]To whom correspondence should be addressed. Email: wu@crystal.harvard.edu.

This article contains supporting information online at www.pnas.org/lookup/suppl/doi:10.1073/pnas.1714386114/-/DCSupplemental.

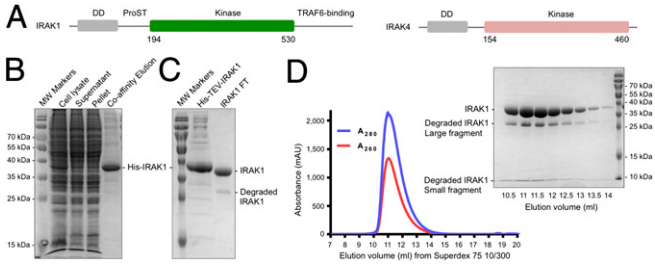

Fig. 1. IRAK1 expression and purification. (*A*) Domain organizations of IRAK1 and IRAK4. DD, death domain; ProST, proline/serine/threonine-rich domain. (*B*) SDS-PAGE of the first-step Co-affinity purification. MW, molecular weight. (*C*) SDS-PAGE of the sample before and after His-tag removal by TEV protease treatment overnight at 4 °C. (*D*) Gel filtration profile of His-tag removed IRAK1 on a Superdex 75 10/300 column and the corresponding SDS-PAGE of the elution fractions. The degraded IRAK1 fragments coeluted with the nondegraded construct band.

Innate immune signaling has an essential role in inflammation, and the dysregulation of signaling components of this pathway is increasingly being recognized as an important factor in cancer initiation, progression, and metastasis, as well as in autoimmunity. However, among the four IRAKs, only the IRAK4 kinase domain structure has been determined, both alone and in complex with various inhibitors (10, 21–30). No structural information is currently available for IRAK1. In this report, we present the crystal structure of the human IRAK1 kinase domain, which provides important insights into inhibitor binding as well as homo- and heterodimerization with IRAK4.

Results

Proteolytic Screen Enables IRAK1 Crystallization and Structure Determination. The construct of the WT IRAK1 kinase domain (residues 194 to 530) (Fig. 1*A*) was designed based on sequence alignment with the published crystallizable construct of the IRAK4 kinase domain (30). It contains an N-terminal His-tag followed by a tobacco etch virus (TEV) cleavage site, and the protein was expressed using a baculovirus-mediated insect cell expression system. After the first-step affinity purification using HisPur Cobalt affinity resin (Fig. 1*B*), the His-tag was removed (Fig. 1*C*), and the protein was further purified by gel filtration (Fig. 1*D*). Initially, we used 150 mM NaCl for the purification, but the protein was not stable and often precipitated. Using differential scanning fluorimetry (31) to assess the IRAK1 melting temperature (T_m) under different solution conditions, we found that a higher salt concentration (500 mM) improved the protein stability (Fig. S1). The molecular mass of the IRAK1 kinase domain construct without the His-tag is 37.3 kDa. The protein was shown as a single peak from the gel filtration profile, with a tendency to degrade into two fragments of about ∼30 kDa and <10 kDa as assessed by sodium dodecyl sulfate polyacrylamide gel electrophoresis (SDS-PAGE). These two fragments comigrated with the full-length construct on gel filtration chromatography (Fig. 1*D*), suggesting that the two fragments are still associated with each other in solution. Extensive crystallization trials failed to produce any crystals, likely due to degradation and the resulting heterogeneity.

Because the two proteolytic fragments comigrated together, as well as with the full-length kinase domain, we attempted to improve the homogeneity of the sample by limited proteolysis to promote crystallization. We screened 12 proteases and found that treatment with clostripain, which cleaves after arginine residues, generated two cleaved products that appeared to migrate on SDS-PAGE at the same positions as the fragments from autodegradation (Fig. 2*A*). Mass spectrometry analysis, together with the molecular weights of the fragments, suggested that the cleavage site by clostripain is R450. Notably, R450 locates near the beginning of a long insertion in IRAK1 (residues 449 to 475) relative to IRAK4. This entire insertion is present in the proteolyzed protein, as shown by peptide mapping using mass spectrometry (Fig. S2), but is partly disordered in the structure.

To enable crystallization, we identified the optimal clostripain: IRAK1 ratio, incubation time, and temperature and carried out crystallization trials with the small-molecule compound JH-I-25 (23). A crystal hit was identified from the Molecular Dimensions PACT screening kit, followed by crystallization optimization. SDS-PAGE of dissolved crystals confirmed that the crystals contained proteolyzed IRAK1 (Fig. 2*B*). JH-I-25 is a dual IRAK1/4 inhibitor, with an IC_{50} of 9.3 nM and 17.0 nM for IRAK1 and IRAK4, respectively, as measured by Invitrogen Lantha (IRAK1) and Z′-LYTE (IRAK4) assays. Differential scanning fluorimetry showed that the compound stabilized IRAK1 by ∼8 °C in Tm, from 45 °C for IRAK1 to 53 °C for the IRAK1/JH-I-25 complex (Fig. S3). Diffraction data were collected to 2.3 Å resolution using synchrotron radiation, and a molecular replacement solution was obtained using an apo-structure of the IRAK4 kinase domain as a model (PDB ID code 2NRU) (Table S1). There are two IRAK1 molecules (chain A and B) per crystallographic asymmetric unit. Subsequent model building and refinement were carried out in Coot (32) and Phenix (33).

Structural Differences Between IRAK1 and IRAK4. The IRAK1 structure in complex with an inhibitor exhibits the canonical two-lobe (N and C lobes) architecture of protein kinases (Fig. 3 *A* and *B*). Similar to IRAK4, an ordered αB helix precedes the kinase domain and packs against the concave surface of the central five-stranded β-sheet of the N-terminal lobe through hydrophobic interactions (Fig. 3 *B* and *C*). The C-lobe is predominantly α-helical. The N- and C-terminal lobes are connected by the hinge region, which partially forms the binding site for ATP. The inhibitor JH-I-25 can be unambiguously modeled in the electron density map and occupies the ATP-binding site (Fig. 3*B*). Although the IRAK1 kinase domain only shares 31% sequence identity with IRAK4, its overall structure is highly similar to that of IRAK4, with root-mean-square deviation (rmsd) values of 1.42 Å over the Cα positions of the 245 corresponding residues in IRAK4 (PDB ID code 2NRU) (30) (Fig. 3*C*). Three regions are disordered in the structure, residues 243 to 247 in chain A and 244 to 248 in chain B at the loop between β3 and αC, residues 367 to 382 within the activation loop, and residues 449 to 460 in A and 449 to 463 in B at the long insertion between αG and αH (Fig. 3*B*). Despite being largely disordered, the IRAK1 activation loop is natively phosphorylated at S373, S375, S376, and T381, as shown by liquid chromatography tandem-mass spectrometry (LC/MS/MS) (Fig. S2). It should be noted that the disordered activation loop (residues 367 to 382) situates away from the inhibitor-binding site (Fig. 3*B*).

IRAK1 shows four major local structural differences from IRAK4 (Fig. 3 *C*–*E*). First, although β1 in IRAK1 aligns well

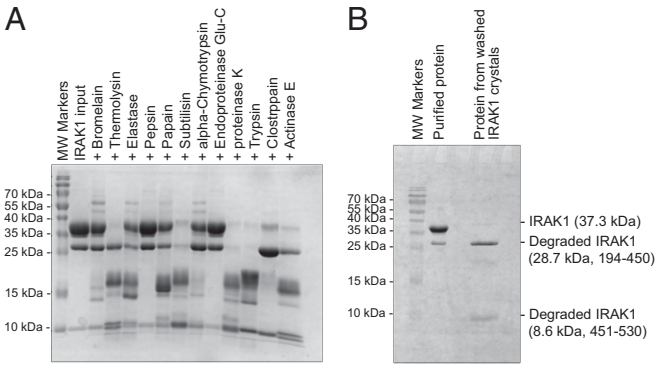

Fig. 2. Proteolytic screening of the IRAK1 kinase domain construct. (*A*) SDS-PAGE of purified IRAK1 treated with various proteases at a 1,000:1 (wt/wt) ratio at 37 °C for 1 h. (*B*) SDS-PAGE of purified IRAK1 before clostripain treatment and IRAK1 from washed crystals.

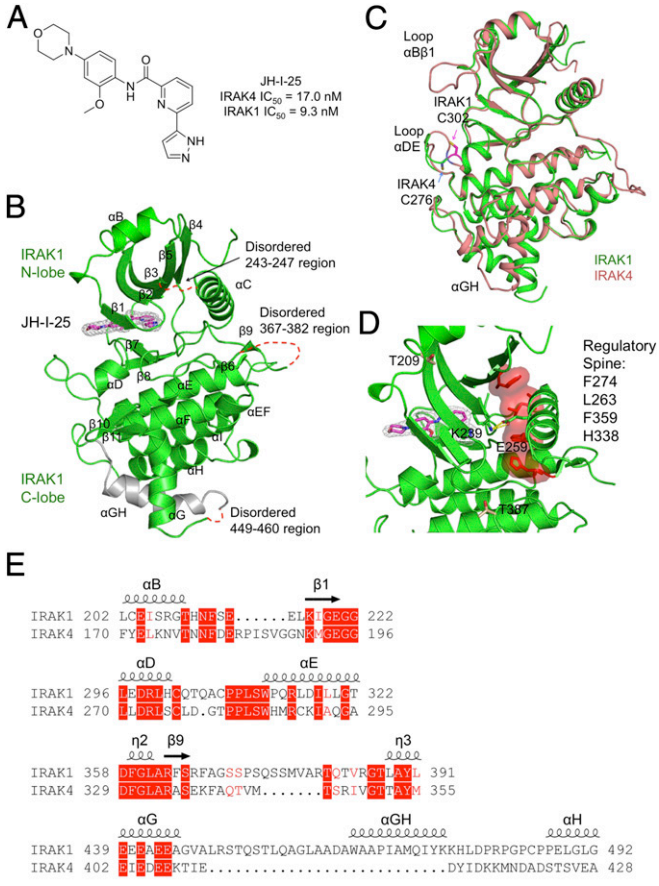

Fig. 3. Structure of inhibitor-bound IRAK1. (*A*) Chemical structure of the dual IRAK1/4 inhibitor JH-I-25 used in the cocrystallization. (*B*) A ribbon diagram of IRAK1 in complex with the inhibitor. The secondary structures are labeled, and the JH-I-25 inhibitor is shown with carbon atoms in magenta, nitrogen atoms in blue, and oxygen atoms in red, superimposed with its electron density in gray. IRAK1 is in green with the exception of the long, gray-colored IRAK1-specific insertion. (*C*) Superposition between IRAK1 (green) and IRAK4 (pink, PDB ID code 2NRU). The main differences between these two kinase domains at the αBβ1 loop, the αDE loop, and the αGH insertion are labeled. The different locations of C302 of IRAK1 and its sequence-conserved counterpart C276 of IRAK4 are indicated. (*D*) The regulatory spine and the K239-E259 salt bridge both indicate an active conformation of IRAK1. (*E*) Sequence alignment between IRAK1 and IRAK4 at four regions with significantly different structures.

with IRAK4, a long loop in IRAK4 (residues 181 to 191) connecting αB and β1 is replaced by a short loop in IRAK1 (residues 213 to 217). This difference leads to a more solvent exposed ATP-binding pocket in comparison with IRAK4. Second, the loop that connects αD with αE in IRAK1 is one residue longer than in IRAK4. Importantly, this loop, together with αD, forms the ATP front pocket. There are two cysteine residues within this loop in IRAK1, C302, and C307, which could be used to develop covalent kinase inhibitors. C302 of IRAK1 is conserved in IRAK4 as C276, but the locations of these residues are significantly different due to conformational differences in the αDE loop (Fig. 3*C*). Residue C307 is conserved between human and murine IRAK1, but residue C302 is not. Third, there is a seven-residue insertion in the IRAK1 activation loop compared with IRAK4, and this region is largely disordered. The most notable change is the extra insertion sequence (residues 447 to 482) after helix αG in IRAK1. While the beginning part of the insertion is disordered in our structure, residues 463 to 476 form a helix, denoted here as αGH.

Previous biochemical data suggested that IRAK1 is sequentially phosphorylated, first at T209 to weakly activate the kinase, and then at T387 to fully activate the kinase (11). Recombinant full-length IRAK1 expressed in insect cells has been reported to be fully phosphorylated (11). In contrast, our construct lacking the DD is not phosphorylated at either T209 or T387. However, the kinase adopts an active conformation, as defined by the presence of an assembled regulatory spine and the salt bridge between K239 of β3 and E259 of αC (Fig. 3*D*). In addition, the recombinant IRAK1 kinase domain showed similar kinase activity as the recombinant IRAK4 kinase domain while the kinase-dead IRAK1 mutant (D340N) did not show any significant kinase activity (Fig. S4*A*). The side chain of T209 formed intimate interactions with surrounding atoms (Fig. S4*B*) and would likely require conformational changes in IRAK1 for phosphorylation to occur. On the other hand, T387 is highly exposed to solvent, and its phosphorylation is unlikely to significantly alter the conformation (Fig. S4*C*). It is unclear why IRAK1 would assume an active conformation in the absence of phosphorylation at T209 and T387. It may be possible that, for the kinase domain alone, such phosphorylation at T209 and T387 is not required for IRAK1 activation. However, in the context of full-length IRAK1, previous data suggest that the N-terminal death domain exerts autoinhibition to the kinase domain (34). Therefore, it remains plausible that T209 and T387 phosphorylation is required to release this autoinhibition.

IRAK1/Inhibitor Interactions. The overall sequence identity among the IRAK family members is ∼30%; however, the residues lining the ATP-binding pocket share 90% identity between IRAK1 and IRAK4. A unique feature of the ATP pocket in the IRAK family is a tyrosine gatekeeper residue (Y288 in IRAK1 and Y262 in IRAK4) (30). In IRAK1, Y288 participates in a polar interaction network with the catalytic lysine K239 from β3, E259 from αG, and D358 from the Asp-Phe-Gly (DFG) motif to stabilize the DFG-in active conformation (Fig. 4*A*). The gatekeeper residue controls access to a preexisting ATP back pocket. A small gatekeeper residue enables inhibitors to access the ATP back pocket to gain more potential selectivity. In the IRAK family, the presence of a bulky tyrosine gatekeeper residue blocks access to this back pocket. Since this tyrosine gatekeeper is exclusive to the IRAK family, it may be explored to develop IRAK family-specific inhibitors.

Indeed, the inhibitor JH-I-25 forms a π–π stacking interaction with the gatekeeper residue Y288 and hydrogen bonds (H-bonds) with the hinge region and the catalytic lysine K239 (Fig. 4*B*). At the back of the ATP pocket, the pyrazole moiety of the inhibitor forms H-bonds with the carboxylate group of D358 and a water molecule, which also forms H-bonds with catalytic K239, gatekeeper Y288, and E259. The amide linker of the inhibitor forms a single H-bond interaction with L291 of the hinge region. The morpholine tail of the inhibitor interacts with a water molecule, which forms H-bonds with D298 and S295. When the IRAK1/JH-I-25 complex structure is superimposed with IRAK4, the critical ligand interacting residues in IRAK1 are conserved in sequence and aligned in structure with IRAK4 (Fig. 4*B* and Fig. S5*A*), clearly explaining why JH-I-25 shows similar potency to both IRAK1 and IRAK4. However, the ATP front pockets are different between IRAK1 and IRAK4 (Fig. S5*B*). The front pocket of IRAK1 is very open while the front pocket of IRAK4 is largely closed (Fig. 4 *C* and *D*). Therefore, IRAK1-specific inhibitors may be obtained by extending the inhibitor further into the front pocket. Additionally, IRAK1 has two Cys residues that may be utilized for the development of covalent, IRAK1-specific inhibitors (Figs. 3*C* and 4*E*).

Unlike the IRAK4 KD, the IRAK1 KD Is a Monomer. Previous data have shown that unphosphorylated IRAK4 forms a dimer and that this dimerization is required for efficient *trans*-autophosphorylation (10). IRAK4 dimerization is affected by the phosphorylation state of the kinase, and phosphorylated IRAK4 is monomeric in solution. To determine whether phosphorylation plays a similar role in IRAK1, we first dephosphorylated the IRAK1 kinase domain with λ-phosphatase. Dephosphorylated IRAK1 was analyzed by LC/MS, and no phosphorylation was detectable in the treated sample. Dephosphorylated IRAK1 showed

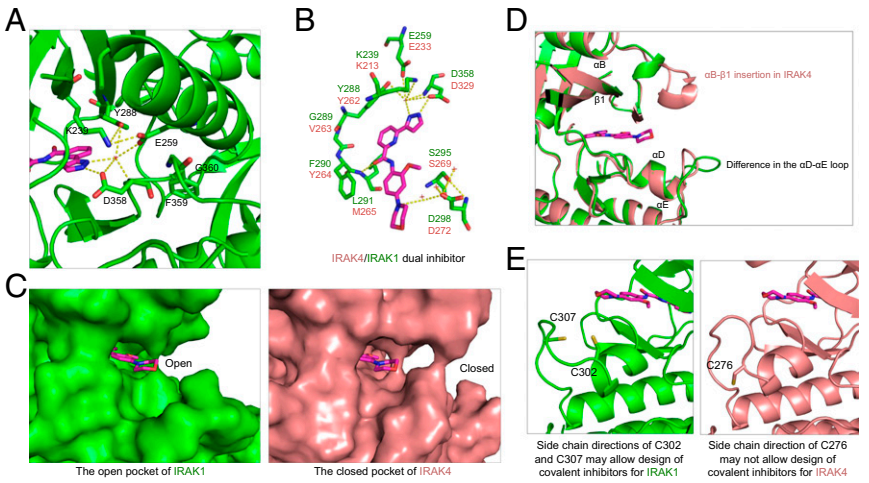

Fig. 4. Detailed mode of inhibitor interaction. (*A*) A hydrogen-bonding network around the IRAK1 gatekeeper residue Y288 near the head of the inhibitor. (*B*) Interactions of IRAK1 with JH-I-25. IRAK1 residues are labeled in green while the corresponding IRAK4 residues are shown in pink. (*C*) Surface diagrams of IRAK1 (*Left*, green) and IRAK4 (*Right*, pink) at the tail of the inhibitor pocket, showing the openness of IRAK1 and closeness of IRAK4. (*D*) Superimposed IRAK1 and IRAK4 at the region of the ATP front pocket showing that an insertion in IRAK4 and distinct loop conformations are responsible for the difference in the openness of this region. (*E*) Side chain directions of C302 and C307 in IRAK1 may allow design of covalent inhibitors, but the side chain direction of C276 of IRAK4 may not.

an experimental molecular mass of 38.9 kDa as measured by multiangle light scattering (MALS), closely approximating the 37.8-kDa theoretical molecular mass of the IRAK1 monomer (Fig. 5*A*). Similarly, both natively and in vitro phosphorylated IRAK1 elutes from a size exclusion column at a position corresponding to monomeric IRAK1 (Fig. 5*A*). Therefore, unlike IRAK4, the IRAK1 kinase domain is monomeric regardless of its phosphorylation state, which is suggestive of a distinct activation mechanism. While IRAK4 dimerization can facilitate its own autophosphorylation and activation (10), IRAK1 activation is dependent on the upstream IRAK4.

To understand why the IRAK1 kinase domain cannot exist as a dimer, we compared the IRAK1 structure with the IRAK4 dimeric structure (PDB ID code 4U97) (10) (Fig. 5 *B* and *C*). In the IRAK4 dimer, a large interaction surface is formed by helix αEF from each monomer and helix αG from one monomer and loop αHI from another monomer, and mutations at the interaction surface dramatically decrease both dimer formation and autophosphorylation. In the IRAK4 dimer, residues L360 and R361 in helix αEF of one monomer contribute to a large buried surface area through both hydrophobic and polar interactions with L360 and Y371 of another monomer. The αEF helix in IRAK1 has a one-residue insertion and swings further out from the C-lobe. When we superimposed two IRAK1 monomers onto the IRAK4 dimer, the αEF helices clashed with each other. The polar interaction was also missing in IRAK1 due to replacing Y371 of IRAK4 with F408 of IRAK1. In addition, the IRAK1 αG helix was shifted by ∼5 Å compared with IRAK4, and would clash with the αH-αI loop from another IRAK1 molecule. Besides the steric hindrance, the highly negatively charged surface on helix αG used in IRAK4 dimerization was not conserved in IRAK1 (Fig. 5*B*). The negatively charged residues in helix αG were substituted with either positively charged or hydrophobic residues although the αH-αI loop has the similar positive charge pattern in comparison with IRAK4. In particular, the charge pair interactions between D398 and K440 and between D405 and K443 in IRAK4 have been replaced by the incompatible K435-R504 and A442-R507 pairs in IRAK1. Together, these observations suggest that IRAK1 is likely incapable of assembling into a face-to-face homodimer similar to that observed for IRAK4.

IRAK1 Heterodimerizes Weakly with Phosphorylated, but Not Unphosphorylated, IRAK4. To determine whether IRAK1 may heterodimerize with IRAK4, we used native PAGE to assess the interaction between the kinase-dead IRAK1 kinase domain (D340N) and both unphosphorylated and phosphorylated full-length IRAK4 (Fig. 6*A*). As with IRAK1 shown in Fig. 1*D*, the recombinant IRAK1 kinase domain protein used here also contained both full-length and degraded fragments. The IRAK1 kinase domain had a high predicted isoelectric point of 8.6 and did not migrate into the resolving gel of the native PAGE alone. Conversely, IRAK4 had a predicted pI of 5.2 and migrated as a distinct band in both its unphosphorylated and phosphorylated forms (Fig. 6*B*). Addition of IRAK1 to unphosphorylated IRAK4 did not alter the migration of IRAK4 in the native PAGE. However, the addition of IRAK1 to phosphorylated IRAK4

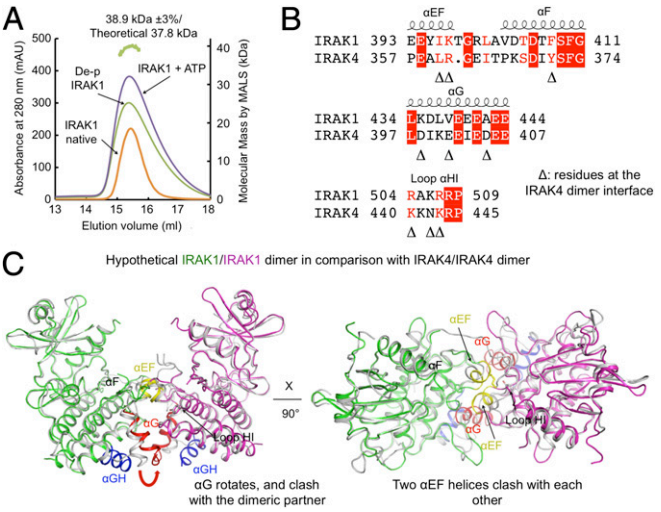

Fig. 5. IRAK1 kinase domain is a monomer in solution in both phosphorylated and unphosphorylated states. (*A*) Gel filtration profiles and multiangle light scattering measurement showed that the IRAK1 kinase domain is a monomer in different states, different from the dimeric state of the IRAK4 kinase domain in the unphosphorylated form. The green track on the top marks the measured molecular mass of the dephosphorylated IRAK1 kinase domain. mAU, absorption units. (*B*) Sequence alignment between IRAK1 and IRAK4 at the IRAK4 dimerization interface. Important IRAK4 dimerization residues are indicated by triangles. (*C*) A model of a hypothetical IRAK1 homodimer would have caused clash in several dimerization elements including the αG and the αEF regions.

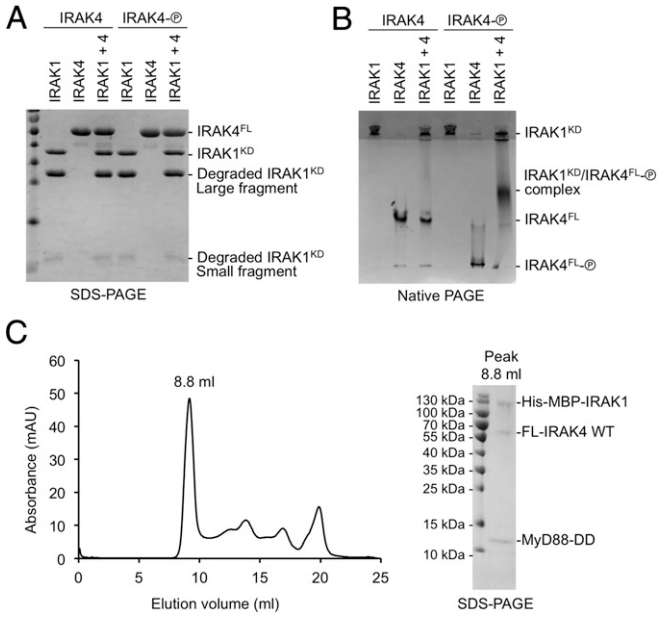

Fig. 6. IRAK1 interacts weakly with phosphorylated IRAK4. (*A*) IRAK1 and two forms of IRAK4, unphosphorylated (left lanes, "IRAK4") and phosphorylated (shown as an encircled P; right lanes, "IRAK4-P") on an SDS-PAGE. (*B*) IRAK1 and two forms of IRAK4, unphosphorylated (left lanes, "IRAK4") and phosphorylated (right lanes, "IRAK4-P") on a native PAGE, showing the shifted band containing IRAK1 and phosphorylated IRAK4. (*C*) Gel filtration profile (*Left*) and SDS-PAGE (*Right*) of the peak fraction for the reconstituted complex of the MyD88 death domain (DD), full-length (FL) IRAK4, and His-MBP–tagged IRAK1 containing the DD and the kinase domain.

resulted in a change in the migration behavior of IRAK4 (Fig. 6*B*). The appearance of this new migrating species was accompanied by a reduction in the amount of IRAK1 present in the top of the gel. As no ATP was present during the native PAGE experiment, the new band likely corresponds to a complex between IRAK1 and phosphorylated IRAK4, rather than any new phosphorylation products.

We propose that this interaction between phosphorylated IRAK4 and IRAK1 occurs most efficiently once unphosphorylated inactive IRAK1 is recruited to the Myddosome through death domain interactions. Because our earlier structure solution was performed on the MyD88/IRAK4/IRAK2 death domain complex (9), we coexpressed MyD88 DD, full-length IRAK4, and the DD and kinase domain region of IRAK1. We found that these three recombinant proteins comigrated on a gel filtration column (Fig. 6*C*), confirming formation of the MyD88/IRAK4/IRAK1 Myddosome. Our data that only the phosphorylated IRAK4 kinase domain interacts with the IRAK1 kinase domain contradict a previous report which detected interaction of overexpressed kinase-dead IRAK4 with death domain deleted IRAK1 in 293T cells (34). However, endogenous IRAK4 is expressed at a high level in 293T cells, which might have phosphorylated overexpressed kinase-dead IRAK4 to enable its interaction with the IRAK1 kinase domain. Consistently, overexpressed kinase-dead IRAK4 did not interact with death domain deleted IRAK1 in RAW 264.7 cells (34).

Discussion

With both IRAK1 and IRAK4 kinase domain structures available, it is now possible to attempt structure-guided design of dual IRAK1/4 or IRAK1- or IRAK4-specific inhibitors. IRAK1 and IRAK4 share a conserved ATP-binding pocket with a unique tyrosine gatekeeper residue, which provides a great opportunity to develop dual IRAK1/IRAK4 inhibitors. Since both IRAK1 and IRAK4 kinases functionally participate in the same signaling pathway, dual kinase inhibitors might provide more robust inhibition of NF-κB signaling in comparison with IRAK1- or IRAK4-specific inhibitors. On the other hand, there is evidence that differential inhibition of IRAK1 or IRAK4 may selectively influence the different downstream pathways that also include MAP kinase activation. With the presence of death domains in these kinases, IRAKs have also been shown to play important scaffolding functions independent of their kinase activities. In this regard, modulation of the death domain interactions may offer an alternative and complementary approach in the development of therapeutics against IRAK-dependent inflammatory outputs.

Recently, IRAK1 activation and overexpression have been reported in myelodysplastic syndrome (MDS) and acute myeloid leukemia (AML) (35), and a high level of IRAK1 expression correlated with reduced overall survival (35). IRAK1 is also overexpressed and hyperphosphorylated in a subset of breast cancers: in particular, triple-negative breast cancer (TNBC) (36). An IRAK1-specific inhibitor could provide a therapeutic treatment for these IRAK1 overexpression and overactivation conditions. Our structure provides several insights into the design of IRAK1-specific inhibitors. First, although it is difficult to distinguish IRAK1 from IRAK4 within the ATP pocket, the region near the front of the ATP pocket is different between IRAK1 and IRAK4 (Fig. 4 *C* and *D*). IRAK1 is open in this region while IRAK4 is more closed in this region, limiting the length of the inhibitors that can be bound to IRAK4. Cysteine residues C302 and C307 of IRAK1, which are adjacent to the ATP pocket, could also be utilized to develop irreversible IRAK1 inhibitors. In contrast, the cysteine residue C276 of IRAK4 has its side chain pointed down, away from the ATP pocket (Figs. 3*C* and 4*E*).

Our studies further reveal mechanisms of kinase activation within the Myddosome (Fig. 7). Upon IL-1 or TLR stimulation, the adaptor protein MyD88, which has TIR and DD protein–protein interaction domains, is recruited to the membrane through TIR–TIR domain interactions. MyD88 then uses its DD to recruit downstream kinases IRAK4 and IRAK1 to form the Myddosome (9). At resting state, cellular concentrations of IRAK4 are low to prevent ligand-independent IRAK4 activation via dimerization, and IRAK1 forms a complex with Tollip to

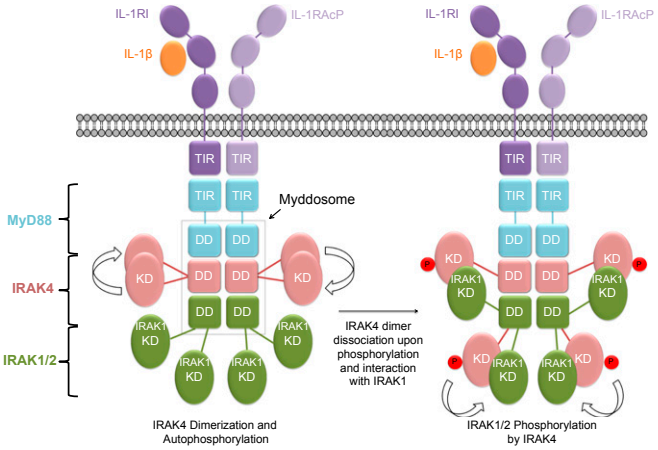

Fig. 7. A schematic diagram of IRAK activation within the Myddosome shown here for the IL-1 receptors. Upon ligand binding, IL-1 receptor (IL-1R) and IL-1 receptor accessary protein (IL-1RAcp) recruit MyD88, which in turn recruits the upstream kinase IRAK4 and then the downstream kinase IRAK1 or IRAK2. IRAK4 recruitment leads to increased local concentration of the kinase domain, leading to its dimerization and *trans*-autophosphorylation. Phosphorylated IRAK4 dissociates from the dimer to interact with and phosphorylate IRAK1 or IRAK2, leading to the first step of its activation.

block IRAK1 phosphorylation. Upon recruitment, the local concentration of IRAK4 is dramatically increased, promoting dimerization, *trans*-autophosphorylation, and activation, with subsequent dissociation of phosphorylated IRAK4 into monomers. Previous data suggest that the IRAK1 kinase domain is autoinhibited by the N-terminal death domain and the C-terminal TRAF6-binding domain through intramolecular interactions (34). Unlike the IRAK4 kinase domain, our data suggest that the IRAK1 kinase domain cannot be activated by homodimerization. Instead, the IRAK1 kinase domain forms a heterodimer with the phosphorylated IRAK4 kinase domain (Fig. 6*B*). Phosphorylation by IRAK4 may then allosterically activate IRAK1 (37), and further IRAK1 autophosphorylation results in full IRAK1 activation and execution of the pathway.

Materials and Methods

Protein Expression and Purification. The human IRAK1 kinase domain (residues 194 to 530) was expressed in insect cell. Protein was purified with HisPur Cobalt Resin (Thermo Scientific) followed by size-exclusion chromatography. For reconstitution of the MyD88/IRAK4/IRAK1 Myddosome, N-terminal His-MBP human IRAK1 (residues 1 to 524), His-tagged human MyD88 death domain (residues 20 to 117), and full-length human IRAK4 were coexpressed in insect cells. The complex was purified with Ni–NTA resin, followed by anion exchange and size-exclusion chromatography. Further details can be found in *SI Materials and Methods*.

Limited Proteolysis Screen. Proteases were purchased from Hampton Research and prepared as stock solutions according to the manufacturer's instructions. For the limited proteolysis screen, 10 μg of recombinant IRAK1 was incubated with 0.01 μg of different proteases at 37 °C for 1 h. The reaction was stopped by adding SDS-PAGE sample buffer, followed by boiling at 95 °C for 10 min. The samples were analyzed by SDS-PAGE.

Crystallization, Data Collection, and Structure Determination. The IRAK1 kinase domain protein was mixed with the JH-I-25 compound at a 1:3 molar ratio, and the mixture was incubated with clostripain at a 1,000:1 molar ratio at room temperature for 1 h before setting up crystallization trays. Crystals were obtained by hanging drop vapor diffusion at 16 °C by mixing equal volumes of the protein and the reservoir solution containing 20% PEG3350, 200 mM $CaCl_2$, 100 mM Hepes at pH 7. Crystals were harvested, cryoprotected with reservoir solution supplemented with 25% (vol/vol) glycerol, and flash-frozen in liquid nitrogen. Data collection was performed at the Advanced Photon Source using Northeastern Collaborative Access Team (NE-CAT) beamlines 24-ID-C and 24-ID-E. Data were processed by XDS (38), and a molecular replacement solution was obtained from Phaser (33) using the IRAK4 kinase domain structure (PDB ID code 2NRU) as a searching model. Subsequent model building and refinement were carried out in Coot (32) and Phenix (33). Structure was validated by Molprobity (39). Figures were generated using PyMOL (40).

Multiangle Light Scattering (MALS). For molecular mass determination by MALS, protein samples were injected into a Superdex 200 (10/300 GL) gel filtration column equilibrated with the gel filtration buffer. The chromatography system was coupled to a three-angle light scattering detector (miniDAWN TRISTAR) and a refractive index detector (Optilab DSP) (Wyatt Technology). Data were collected every 0.5 s with a flow rate of 0.5 mL/min. Data analysis was carried out using ASTRA V.

ACKNOWLEDGMENTS. We thank the Northeastern Collaborative Access Team (NE-CAT) staff for their assistance in data collection. This work is based upon research conducted at the NE-CAT beamlines, which are funded by the National Institute of General Medical Sciences from the National Institutes of Health (P41 GM103403). The Pilatus 6M detector on the 24-ID-C beamline is funded by NIH-Office of Research Infrastructure Programs High-End Instrumentation Grant S10 RR029205. This research used resources of the Advanced Photon Source, a US Department of Energy (DOE) Office of Science User Facility operated for the DOE Office of Science by Argonne National Laboratory under Contract DE-AC02-06CH11357. We acknowledge support from National Institutes of Health Grant AI050872 (to H.W.) and the Cancer Research Institute (Q.Q.).

1. Cao Z, Henzel WJ, Gao X (1996) IRAK: A kinase associated with the interleukin-1 receptor. *Science* 271:1128–1131.
2. Muzio M, Ni J, Feng P, Dixit VM (1997) IRAK (Pelle) family member IRAK-2 and MyD88 as proximal mediators of IL-1 signaling. *Science* 278:1612–1615.
3. Wesche H, et al. (1999) IRAK-M is a novel member of the Pelle/interleukin-1 receptor-associated kinase (IRAK) family. *J Biol Chem* 274:19403–19410.
4. Li S, Strelow A, Fontana EJ, Wesche H (2002) IRAK-4: A novel member of the IRAK family with the properties of an IRAK-kinase. *Proc Natl Acad Sci USA* 99:5567–5572.
5. Ye H, et al. (2002) Distinct molecular mechanism for initiating TRAF6 signalling. *Nature* 418:443–447.
6. Wesche H, Henzel WJ, Shillinglaw W, Li S, Cao Z (1997) MyD88: An adapter that recruits IRAK to the IL-1 receptor complex. *Immunity* 7:837–847.
7. O'Neill LA, Bowie AG (2007) The family of five: TIR-domain-containing adaptors in Toll-like receptor signalling. *Nat Rev Immunol* 7:353–364.
8. Burns K, et al. (2000) Tollip, a new component of the IL-1RI pathway, links IRAK to the IL-1 receptor. *Nat Cell Biol* 2:346–351.
9. Lin SC, Lo YC, Wu H (2010) Helical assembly in the MyD88-IRAK4-IRAK2 complex in TLR/IL-1R signalling. *Nature* 465:885–890.
10. Ferrao R, et al. (2014) IRAK4 dimerization and trans-autophosphorylation are induced by Myddosome assembly. *Mol Cell* 55:891–903.
11. Kollewe C, et al. (2004) Sequential autophosphorylation steps in the interleukin-1 receptor-associated kinase-1 regulate its availability as an adapter in interleukin-1 signaling. *J Biol Chem* 279:5227–5236.
12. Cao Z, Xiong J, Takeuchi M, Kurama T, Goeddel DV (1996) TRAF6 is a signal transducer for interleukin-1. *Nature* 383:443–446.
13. Hemmi H, et al. (2000) A Toll-like receptor recognizes bacterial DNA. *Nature* 408:740–745.
14. Hemmi H, et al. (2002) Small anti-viral compounds activate immune cells via the TLR7 MyD88-dependent signaling pathway. *Nat Immunol* 3:196–200.
15. Uematsu S, et al. (2005) Interleukin-1 receptor-associated kinase-1 plays an essential role for Toll-like receptor (TLR)7- and TLR9-mediated interferon-alpha induction. *J Exp Med* 201:915–923.
16. Zhang G, Ghosh S (2002) Negative regulation of toll-like receptor-mediated signaling by Tollip. *J Biol Chem* 277:7059–7065.
17. Strelow A, Kollewe C, Wesche H (2003) Characterization of Pellino2, a substrate of IRAK1 and IRAK4. *FEBS Lett* 547:157–161.
18. Smith H, et al. (2009) Identification of the phosphorylation sites on the E3 ubiquitin ligase Pellino that are critical for activation by IRAK1 and IRAK4. *Proc Natl Acad Sci USA* 106:4584–4590.
19. Ordureau A, et al. (2008) The IRAK-catalysed activation of the E3 ligase function of Pellino isoforms induces the Lys63-linked polyubiquitination of IRAK1. *Biochem J* 409:43–52.
20. Goh ET, et al. (2012) Identification of the protein kinases that activate the E3 ubiquitin ligase Pellino 1 in the innate immune system. *Biochem J* 441:339–346.
21. Lee KL, et al. (2017) Discovery of clinical candidate 1-[(2S,3S,4S)-3-ethyl-4-fluoro-5-oxopyrrolidin-2-yl]methoxy-7-methoxyisoquinoline-6-carboxamide (PF-06650833), a potent, selective inhibitor of interleukin-1 receptor associated kinase 4 (IRAK4), by fragment-based drug design. *J Med Chem* 60:5521–5542.
22. Kuglstatter A, et al. (2007) Cutting edge: IL-1 receptor-associated kinase 4 structures reveal novel features and multiple conformations. *J Immunol* 178:2641–2645.
23. Buckley GM, et al. (2008) IRAK-4 inhibitors. Part 1: A series of amides. *Bioorg Med Chem Lett* 18:3211–3214.
24. Hanisak J, et al. (2016) Efforts towards the optimization of a bi-aryl class of potent IRAK4 inhibitors. *Bioorg Med Chem Lett* 26:4250–4255.
25. McElroy WT, et al. (2015) Potent and selective amidopyrazole inhibitors of IRAK4 that are efficacious in a rodent model of inflammation. *ACS Med Chem Lett* 6:677–682.
26. Lim J, et al. (2015) Discovery of 5-Amino-N-(1H-pyrazol-4-yl)pyrazolo[1,5-a]pyrimidine-3-carboxamide inhibitors of IRAK4. *ACS Med Chem Lett* 6:683–688.
27. McElroy WT, et al. (2015) Discovery and hit-to-lead optimization of 2,6-diaminopyrimidine inhibitors of interleukin-1 receptor-associated kinase 4. *Bioorg Med Chem Lett* 25:1836–1841.
28. Seganish WM, et al. (2015) Discovery and structure enabled synthesis of 2,6-diaminopyrimidin-4-one IRAK4 inhibitors. *ACS Med Chem Lett* 6:942–947.
29. Smith GF, et al. (2017) Identification of quinazoline based inhibitors of IRAK4 for the treatment of inflammation. *Bioorg Med Chem Lett* 27:2721–2726.
30. Wang Z, et al. (2006) Crystal structures of IRAK-4 kinase in complex with inhibitors: A serine/threonine kinase with tyrosine as a gatekeeper. *Structure* 14:1835–1844.
31. Niesen FH, Berglund H, Vedadi M (2007) The use of differential scanning fluorimetry to detect ligand interactions that promote protein stability. *Nat Protoc* 2:2212–2221.
32. Emsley P, Lohkamp B, Scott WG, Cowtan K (2010) Features and development of Coot. *Acta Crystallogr D Biol Crystallogr* 66:486–501.
33. Adams PD, et al. (2010) PHENIX: A comprehensive Python-based system for macromolecular structure solution. *Acta Crystallogr D Biol Crystallogr* 66:213–221, Version 1.8.4-1496.
34. Nguyen T, De Nardo D, Masendycz P, Hamilton JA, Scholz GM (2009) Regulation of IRAK-1 activation by its C-terminal domain. *Cell Signal* 21:719–726.
35. Rhyasen GW, et al. (2013) Targeting IRAK1 as a therapeutic approach for myelodysplastic syndrome. *Cancer Cell* 24:90–104.
36. Wee ZN, et al. (2015) IRAK1 is a therapeutic target that drives breast cancer metastasis and resistance to paclitaxel. *Nat Commun* 6:8746, and erratum (2015) 6:10054.
37. Vollmer S, et al. (2017) The mechanism of activation of IRAK1 and IRAK4 by interleukin-1 and Toll-like receptor agonists. *Biochem J* 474:2027–2038.
38. Kabsch W (2010) Xds. *Acta Crystallogr D Biol Crystallogr* 66:125–132.
39. Chen VB, et al. (2010) MolProbity: All-atom structure validation for macromolecular crystallography. *Acta Crystallogr D Biol Crystallogr* 66:12–21, Version 4.1.
40. Delano WL (2002) The PyMOL molecular graphics system (Schrödinger LLC, San Carlos, CA), Version 0.99rc6.